Physics of Fluids

Variations with Mach number for gust–airfoil interaction noise ⊘

Shujie Jiang (蒋树杰) ✉ iD ; Yanan Wang (王亚南); Zhenguo Yan (燕振国); Rongping Zhang (章荣平); Zhiwei Hu (胡志伟) iD
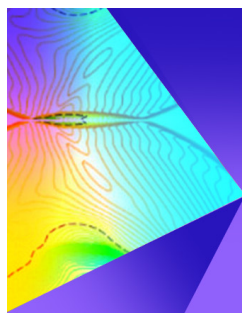
Check for updates

View Online   Export Citation   CrossMark

Physics of Fluids

Special Topic: Shock Waves

Submit Today!

AIP Publishing

Variations with Mach number for gust–airfoil interaction noise

View Online   Export Citation   CrossMark

Shujie Jiang (蒋树杰),[1,2,a] (iD) Yanan Wang (王亚南),[3] Zhenguo Yan (燕振国),[4] Rongping Zhang (章荣平),[1]
and Zhiwei Hu (胡志伟)[2] (iD)

AFFILIATIONS

[1]Laboratory of Aerodynamic Noise Control, China Aerodynamics Research and Development Center, Mianyang,
 Sichuan 621000, People's Republic of China
[2]Faculty of Engineering and Physical Sciences, University of Southampton, Southampton SO17 1BJ, United Kingdom
[3]School of Mechanical Engineering, Xi'an Jiaotong University, Xi'an, Shaanxi 710049, People's Republic of China
[4]State Key Laboratory of Aerodynamics, Mianyang, People's Republic of China

[a]Author to whom correspondence should be addressed: jiangshujie@cardc.cn

ABSTRACT

The interaction of turbulence with airfoil is an important noise source in many engineering fields, including helicopters, turbofans, and contra-rotating open rotor engines, where turbulence generated in the wake of upstream blades interacts with the leading edge of downstream blades and produces aerodynamic noise. One approach to study turbulence–airfoil interaction noise is to model the oncoming turbulence as harmonic gusts. A compact noise source produces a dipole-like sound directivity pattern. However, when the acoustic wavelength is much smaller than the airfoil chord length, the airfoil needs to be treated as a non-compact source, and the gust–airfoil interaction becomes more complicated and results in multiple lobes generated in the radiated sound directivity. Capturing the short acoustic wavelength is a challenge for numerical simulations. In this work, simulations are performed for gust–airfoil interaction at different Mach numbers using a high-fidelity direct computational aeroacoustic (CAA) approach based on a spectral/hp element method verified by a CAA benchmark case. It is found that the squared sound pressure varies approximately as the fifth power of Mach number, which changes slightly with the observer location. This scaling law can give a better sound prediction than the flat-plate theory for thicker airfoils. Furthermore, another prediction method, based on the flat-plate theory and CAA simulation, has been proposed to give better predictions than the scaling law for thicker airfoils.

Published under an exclusive license by AIP Publishing. https://doi.org/10.1063/5.0139656

I. INTRODUCTION

Rotating machinery is essential for air transportation to provide power for aircraft. The noise generated by aircraft has become a more focused environmental concern as governments and international organizations have introduced more strict restrictions on noise pollution, which requires almost double noise reduction every 15 years.[1] For example, NASA suggests a 42 dB noise reduction for aircraft by 2025 in their Environmentally Responsible Aviation project.[2] To meet those restrictions, the aviation industry puts more effort into reducing aircraft noise.

Turbulence–airfoil interaction noise is a significant broadband noise source in rotating machinery, such as helicopter blades,[3] turbofan engines,[4] and contra-rotating open rotors.[5] In these applications, turbulence in the wake of upstream blades interacts with the leading edge of downstream blades. Tonal noise was believed to be dominant compared to broadband noise. However, turbulence–airfoil interaction noise is significant, especially above frequencies of 400 Hz on 1/3

octave sound pressure levels of a contra-rotating open rotor.[6] A later study extended this finding to various contra-rotating open rotor configurations and operating conditions.[7] Therefore, it is crucial to study the mechanisms of the turbulence–airfoil interaction noise to meet the needs for future low-noise aircraft design.

Modeling turbulence is the first step to studying turbulence–airfoil interaction noise. The most common method is using a superposition of harmonic gusts to obtain a synthetic turbulence flow.[8] This method is based on the idea that turbulence can be transformed into a summation of Fourier modes. Therefore, the turbulence–airfoil interaction is simplified to a gust–airfoil interaction process. Generally, gusts are vortical waves with zero dilatation convected by a background mean flow. Gust–airfoil interaction is a simplified model to study turbulence–airfoil interaction noise. It helps to improve the understanding of the mechanisms. Gust–airfoil interaction noise is studied widely by analytical methods[9–11] and numerical simulations.[12,13]

Sears[14] was the first to develop an analytical model to study the lift and moment of an airfoil interacting with a harmonic vortical gust. Amiet[15] extended Sears's model by considering the noise generation of turbulence interacting with an infinite thin flat plate, which became the basis of analytical models to predict turbulence–airfoil interaction noise. However, the geometry effect of an actual airfoil is neglected in Amiet's theory. Later, researchers studied the impact of geometry parameters, such as airfoil thickness, leading edge radius, camber, and angle of attack (AoA). Paterson and Amiet[16] observed noise reduction in high frequencies for thick airfoils in their experiments. Atassi et al.[17] found the acoustic pressure pattern strongly depends on the value of the reduced frequency and the mean-flow Mach number. Gill et al.[13] studied the effect of airfoil thickness and leading edge radius using a computational aeroacoustic (CAA) method. They found the dominant noise reduction mechanism is the distortion of the vortical gusts near the leading edge stagnation region, which smoothed the gust wavefront and reduced its amplitude. Paterson and Amiet[18] showed that the AoA influence for isotropic turbulence-induced noise is small but measurable. Devenport et al.[19] found the effect of AoA is small because of the averaging effect of the isotropic turbulence spectrum. They pointed out that the impact of AoA can be significant in non-isotropic turbulence. Zhong et al.[20] proposed useful corrections to the flat-plate solution to account for the effect of nonuniform mean flows of real airfoils. Huang[21] developed an analytical model by incorporating Fourier transform into the Wiener–Hopf method to elucidate the possible physical mechanisms. Celik et al.[22] performed a comprehensive mapping of wall-pressure fluctuations over an airfoil under different inflow conditions, including a grid-generated turbulent inflow. They found the unsteady airfoil response patterns for the tripped boundary layer and turbulence ingestion cases are dramatic differences compared to smooth inflow conditions. It is difficult to generate an ideal gust in a wind tunnel experiment, so almost all the early researchers used grid-generated turbulence to study the aerodynamic or aeroacoustic response in their experiments. Yang et al.[23] generated a sinusoidal streamwise gust by a multiple-fan array to study the gust–airfoil interaction. They found the fluctuation in the lift force reduces very much at the high frequency, which can be attributed to a significant reduction in the fluctuating pressure difference over the front half of the airfoil. Different from the method used by Yang et al.,[23] Wang and Feng[24] also generated vertical and longitudinal gusts by two pitching airfoils in a low-speed water tunnel. They found that the pitching airfoil can generate vertical gusts when two airfoils pitch in phase. Otherwise, longitudinal gusts generate when the two airfoils pitch out of phase. Wu et al.[25] studied the Sears and Atassi transfer functions at low frequencies by both wind tunnel experiments and numerical simulations. They also established a scaling law for fast determination of the oscillation parameters of the vanes to generate a specific gust angle. Poudel et al.[26] investigated the impact of vertical gusts on stationary and oscillating NACA0012 airfoils at low Reynolds numbers. The pitch-down maneuver and oscillating airfoil motion were tested as methods for mitigating the effects of gusts. They found that increasing the reduced frequency of the oscillating airfoil can dominate the gust and results in a predictable oscillatory lift and drag/thrust behavior. Seo et al.[27] proposed an aeroacoustic partitioning method to decompose the loading noise into the components associated with vortex structures, which can attribute to the sound generation mechanism. Recently, the wavy leading edge has been found to be a useful technology for noise reduction. Narayanan et al.[28] performed an experimental investigation for the noise reduction generated by turbulence airfoil interaction with a wavy leading edge. Noise reductions are found to be significantly higher for the flat plates with a maximum noise reduction of around 9 dB compared with about 7 dB for the airfoil. They concluded the amplitude of the wavy leading edge was a key parameter. Tian and Lyu[29] developed an analytical method to predict the broadband trailing-edge noise for rotating serrated blades. Noise reduction can be found in the intermediate- and high-frequency ranges at low Mach numbers by using trailing-edge serrations. However, they also found the noise increase in the intermediate-frequency range at high Mach numbers. This indicates the effect of the Mach number can be important.

The flow changes significantly along the blade from the root to the tip, resulting in a wide range of Mach numbers on the blade surface. The intensity of sound can be increased due to the supersonic flow near the tip of helicopter blades. So the gust–airfoil interaction can be affected by the wide range of Mach number distribution. In a typical gust–airfoil interaction process, the wavelength of generated acoustic waves depends on both the gust wavelength and the mean-flow Mach number. When the wavelength of a generated acoustic wave is much larger than the chord of the airfoil, the airfoil can be treated as a compact noise source and produces a dipole-like sound directivity. This situation happens when the gust frequency or the free stream Mach number is small. The far-field sound is found to scale as the sixth power of the Mach number.[30] Contrarily, when a high-frequency gust interacts with an airfoil in a relatively high Mach number flow, the wavelength of the generated sound is small compared with the airfoil chord. Therefore, the noise sources on the airfoil are non-compact. The directivity of the radiated sound becomes more complex due to sound scattering. There is little research on the scaling law for gust–airfoil interaction noise, especially for non-compact sources. Similar research can be found given by Singer et al.[31] They studied the scaling law for the sound generated by vortices passing over a sharp trailing edge. They found the mean square pressure varies as $Ma^{5.2}$ and the exponent changes slightly with the observer angle.

This paper presents a high-order and high-fidelity CAA simulation based on the spectral/hp element method.[32] The simulation method is verified by a benchmark case[33] and the flat-plate theory.[15] The scaling law for gust–airfoil interaction noise is studied using the CAA simulation results. The scaled sound pressure is compared with the CAA simulation and the flat-plate theory. This paper is organized as follows. The numerical method is presented in Sec. II, followed by its validation as shown in Sec. III. In Sec. IV, the scaling law for gust–airfoil interaction is introduced in detail. Variations of sound pressure with different Mach numbers and angles of observers are studied in this section. The scaling law is used to predict the sound pressure for different Mach numbers in Sec. V. Another sound pressure prediction method is proposed based on the flat-plate theory and CAA results, as shown in Sec. VI. In Sec. VII, we summarize the conclusions and give suggestions about the usage of the scaling law for gust–airfoil interaction.

II. NUMERICAL METHOD

The noise generation of gust–airfoil interaction is taken as an inviscid phenomenon; therefore, viscous terms can be excluded.[10] We

consider a two-dimensional compressible inviscid flow, which is governed by the Euler equations

$$\frac{\partial \boldsymbol{u}}{\partial t} + \frac{\partial \boldsymbol{f}_{i,1}}{\partial x_1} + \frac{\partial \boldsymbol{f}_{i,2}}{\partial x_2} = 0, \tag{1}$$

where $\boldsymbol{u}$ is a vector of the conserved variables, and $\boldsymbol{f}_{i,1} = \boldsymbol{f}_{i,1}(\boldsymbol{u})$ and $\boldsymbol{f}_{i,2} = \boldsymbol{f}_{i,2}(\boldsymbol{u})$ are the inviscid fluxes,

$$\boldsymbol{u} = \begin{Bmatrix} \rho \\ \rho u \\ \rho v \\ E \end{Bmatrix}, \quad \boldsymbol{f}_{i,1} = \begin{Bmatrix} \rho u \\ p + \rho u^2 \\ \rho u v \\ u(E+p) \end{Bmatrix}, \quad \boldsymbol{f}_{i,2} = \begin{Bmatrix} \rho v \\ \rho u v \\ p + \rho v^2 \\ v(E+p) \end{Bmatrix}. \tag{2}$$

Here, ρ is the density, u and v are the velocity components in the x_1 and x_2 directions, p is the pressure, and E is the total energy. Throughout this work, we consider a perfect gas for which the pressure is related to the total energy by the following expression:

$$E = \frac{p}{\gamma - 1} + \frac{1}{2}\rho(u^2 + v^2), \tag{3}$$

where γ is the ratio of specific heat.

The equations were discretized following the spectral/hp method using the discontinuous Galerkin (DG) approach presented by Karniadakis and Sherwin.[34] The classical fourth-order Runge–Kutta method[35] is used to advance the simulation in time. All the simulations shown here are performed by the compressible solver within spectral/hp element code Nektar++.[36] Generally, the DG method starts with using a test function to express the governing equations and is integrated over the domain. The DG discretization then allows selecting both a basis of polynomials that represent the solution locally on each element and a set of quadrature points on which the inner products arising in the variational formulation can be calculated. In this paper, the spatial domain is split into quadrilateral elements, and high-order Lagrange tensor-product polynomial shape functions are used in each macro-element. The spatial resolution is controlled by varying the element size or the order of the polynomial, which is interpolated at the Gauss–Lobatto–Legendre quadrature.[36]

III. VALIDATION OF THE SPECTRAL/HP ELEMENT METHOD

The spectral/hp element approach used in this paper is first validated by a benchmark case from the fourth computational aeroacoustics workshop on benchmark problems[33] to test its ability to predict accurately the unsteady aerodynamic and aeroacoustic response of a single airfoil interacting with a two-dimensional gust.

The Joukowski airfoil is chosen with a thickness of $0.12c$ and a camber of $0.02c$ at an angle of attack $\alpha = 2°$, where c is the airfoil chord length. The upstream velocity is given by

$$\boldsymbol{U} = U_\infty \boldsymbol{i} + \boldsymbol{a} \cos\left[\boldsymbol{k}(\boldsymbol{x} - \boldsymbol{i}U_\infty t)\right], \tag{4}$$

where $\boldsymbol{x} = (x_1, x_2)$ denotes the spatial coordinates, $\boldsymbol{a} = (a_1, a_2)$ is the gust amplitude vector with $a_1 = -\epsilon U_\infty k_2/|\boldsymbol{k}|$, $a_2 = -\epsilon U_\infty k_1/|\boldsymbol{k}|$. $\boldsymbol{k}$ is the wavenumber vector, and ϵ is a small parameter satisfying $\epsilon \ll 1$. The governing equations are the two-dimensional compressible Euler equations, as given in Sec. II. The following are the reference values used for non-dimensionalization:

$$L_{ref} = \frac{c}{2}; \quad u_{ref} = U_\infty, \quad \rho_{ref} = \rho_\infty; \quad p_{ref} = \rho_\infty U_\infty^2. \tag{5}$$

A two-dimensional gust with $k_1 = k_2 = 1$ and $\epsilon = 0.02$ is chosen to solve the gust response problem. The freestream Mach number is 0.5.

A second-order modified hierarchical Legendre basis polynomial expansion is used for the spectral/hp element method.[37] The required mesh resolution can be estimated by the "1% rule" given by Moura et al.[38] In their study, the dispersion and diffusion characteristics of a DG simulation are performed to quantify the effective resolution that a given simulation setting can provide. The 1% rule is measured in terms of the largest wavenumber that can be accurately resolved to within a tolerance of 1%.

In this case, the second-order expansion used in this case can resolve, with an error below 1%, non-dimensional wavelengths of

$$\lambda_{min} = \frac{2\pi h_{max}}{|kh|_{1\%}} \tag{6}$$

with $|kh|_{1\%} = 2.616$ (Ref. 38). h_{max} is the maximum mesh size that can be used. For this problem, the minimal wavelength of acoustic waves (propagate to the upstream) is the same as the wavelength of gust $\lambda = \frac{2\pi u}{\omega} = 2\pi$, for $k_1 = k_2 = 1$. In our mesh, the largest non-dimensional element size in the computation domain is 1, which is smaller than the value calculated by the 1% rule. This guarantees the gust and acoustic waves can be calculated accurately.

Sponge layers are used to minimize reflection on all four edges of the computational domain. The length and damping factor of sponge layers are represented by L_s and σ_0. In our study, the length of sponge layers is the same in all directions. The physical domain size is represented by L_p. Within each sponge layer, damping terms are applied as given in Ref. 32,

$$\sigma(x,y) = \frac{\sigma_0\{1 + \cos[\pi A(x)B(y)]\}}{2}, \tag{7}$$

where

$$x \in [x_{min}, x_{max}] \quad \text{and} \quad y \in [y_{min}, y_{max}] \tag{8}$$

with

$$\begin{cases} A(x) = 1 - \max\left[1 - (x - x_{min})/L_s, 0\right] \\ \qquad - \max\left[1 - (x_{max} - x)/L_s, 0\right], \\ B(y) = 1 - \max\left[1 - (y - y_{min})/L_s, 0\right] \\ \qquad - \max\left[1 - (y_{max} - y)/L_s, 0\right]. \end{cases} \tag{9}$$

This approach is ideal for forcing the flow variables to the reference value in the sponge layer to reduce potential reflections from the boundaries to guarantee clean acoustic solutions.[39]

The simulation is performed in a square domain with the airfoil at the center. The computational domain and mesh are presented in Fig. 1. The mesh is generated by an open-source finite element mesh generator Gmsh, which can generate a high-order curved mesh [shown in Fig. 1(b)] that conforms to the computer aided design (CAD) model geometry.[40] The sponge layer is in the outer region [presented in Fig. 1(a)] of the domain with a non-dimensional length $L_s = 9c$ and $\sigma_0 = -1$. The mesh resolution in the sponge layer is the same with the largest non-dimensional element size calculated by the 1% rule. The profile of the sponge layer is kept the same in this part.
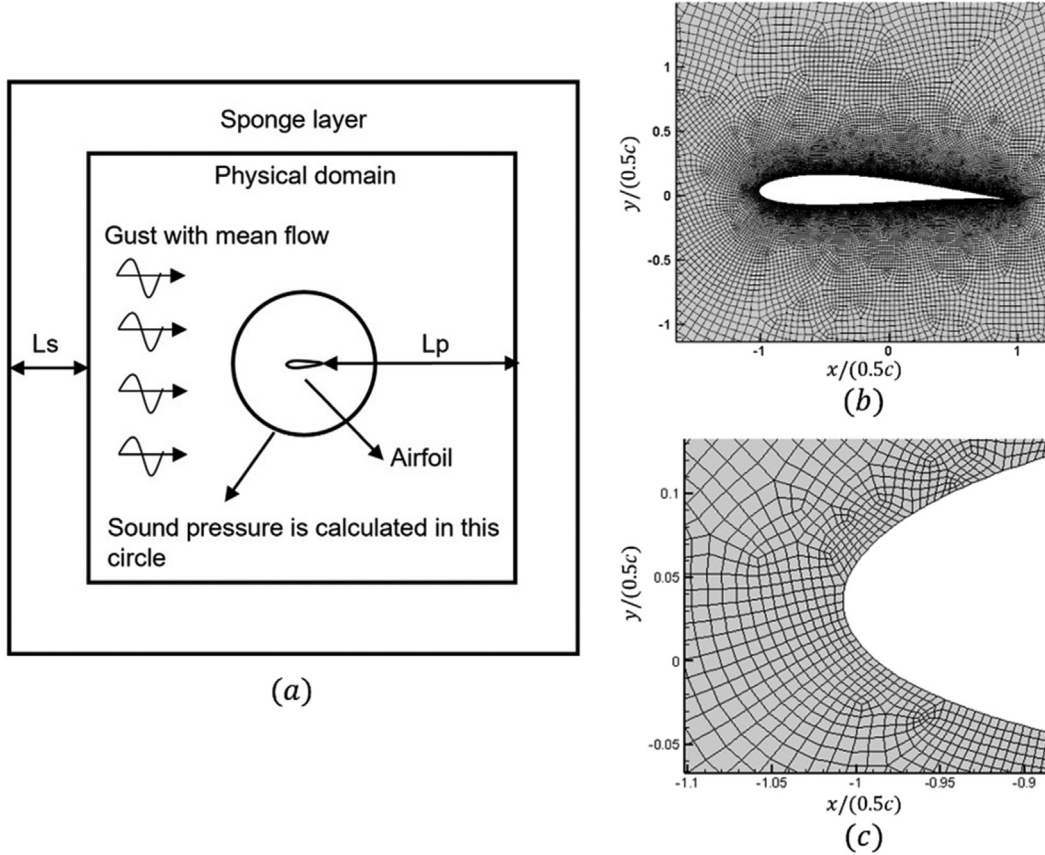
FIG. 1. Example of two-dimensional mesh used in the current study. (a) The sketch of the computational domain. (b) The mesh near the airfoil. (c) The zoomed-in view near the leading edge.

A circle is located at a radius of $4c$ to get the acoustic pressure for comparison with reference data.

Different domain sizes (controlled by L_p), different mesh resolutions (change the minimum mesh size on the airfoil surface), and different data sampling times (one gust period and two gust periods) have been considered for testing the correlation and dependence. Detailed parameters can be found in Table I. The time step is estimated by the definition of the Courant–Friedrichs–Lewy (CFL) number,[41]

$$CFL = \frac{c_\lambda \Delta t \left(a + \sqrt{u_k u_k} \right) P^2}{d_{RK} \Delta x}, \quad (10)$$

where $c_\lambda = 0.2$, $d_{RK} = 2$, and a is the speed of sound, which ensures the maximum stable CFL is almost constant for different values of the polynomial order P. Δt is the time step, Δx is the maximum mesh size, and u_k is the velocity component.

In our case, the simulation is performed for about 100 gust periods using a time step of 1×10^{-4} to avoid spurious solutions in the early stage of the simulation. When the time-averaged pressure changes within an error threshold (10^{-7}, non-dimensionalized by $\rho_\infty U_\infty^2$), the simulation is deemed fully converged, after which the time-averaged pressure on the airfoil surface is calculated during one gust period.

For gusts with wavenumber $k_1 = k_2 = 1$, time-averaged pressure ($\langle p_{wall} \rangle$) and root-mean-squared (RMS) pressure,

TABLE I. The parameters for different cases ($k = 1$, $Ma = 0.5$). The time step is non-dimensionalized by $\frac{c}{2}/U_\infty$.

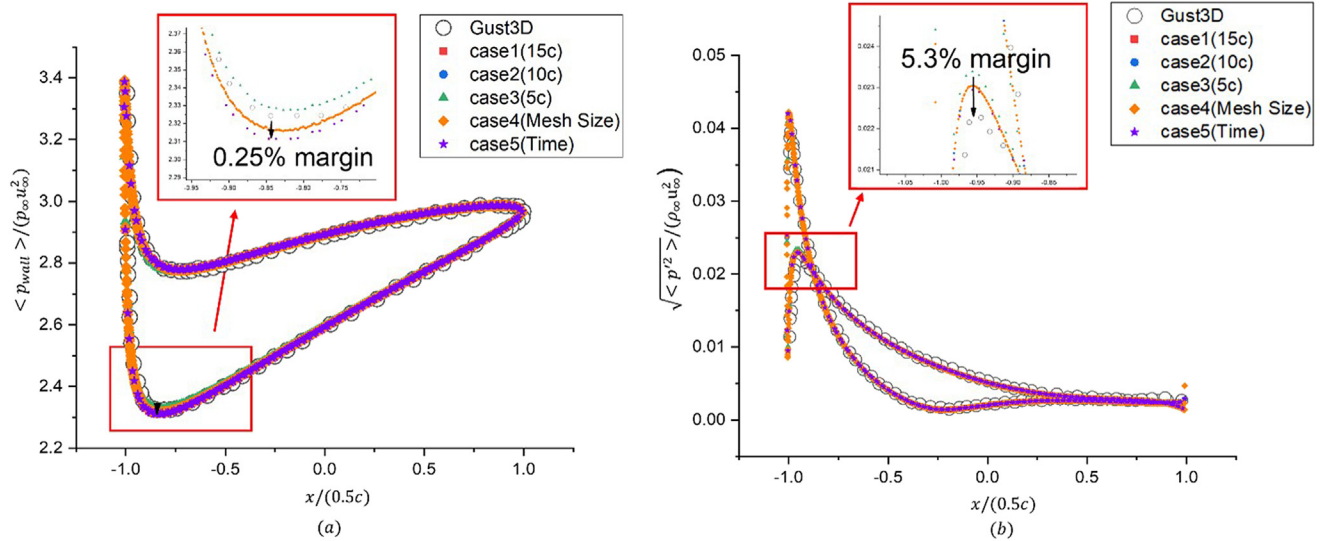| No.	L_p	Airfoil mesh size	Mesh number	Time step	Data collection time	Purpose
1	15c	0.005c	20 849	1×10^{-4}	1 period	Domain size
2	10c	0.005c	14 673	1×10^{-4}	1 period	Domain size
3	5c	0.005c	11 186	1×10^{-4}	1 period	Domain size
4	10c	0.0005c	64 484	5×10^{-5}	1 period	Mesh resolution
5	10c	0.005c	14 673	1×10^{-4}	2 period	Data collection time

FIG. 2. (a) Mean pressure distributions and (b) RMS pressure on the airfoil surface.

$\sqrt{\langle p'^2 \rangle}$ $(p' = p - \langle p \rangle)$, distributions on the airfoil surface are presented in Fig. 2, compared with benchmark reference values from Wang et al.[42] There is a very small difference near the peak between current simulation results and reference data, about 0.25% at the peak of mean pressure and 5.3% for RMS pressure. Above all, a very good agreement is obtained.

The acoustic properties can be represented by the average squared sound pressure $\langle p'^2 \rangle$ measured on a circle. The center of the circle is in the airfoil center, and the radius is defined by $R = \sqrt{(x^2 + y^2)}$, which equals one chord length here. The azimuth is defined by $\theta = \arctan(x/y)$. Figure 3 shows the product by the average

squared sound pressure and the trigonometric function of azimuth. They show a good agreement with the reference data.[42] There is some fluctuation for the smallest domain size (case 3). This may be caused by the fact that the points on the circle with a four-chord length radius are very close to the boundary of the sponge layer. For the cases with bigger domain sizes, the fluctuation seems smaller and gives better results. This indicates that a $10c$ domain size is suitable for our simulation.

Extensive parametric tests of the resolution have been performed to check the influence on aerodynamics and aeroacoustics.[43] Different orders of the basis polynomial expansions are used for the resolution test because using higher-order polynomials along with coarser
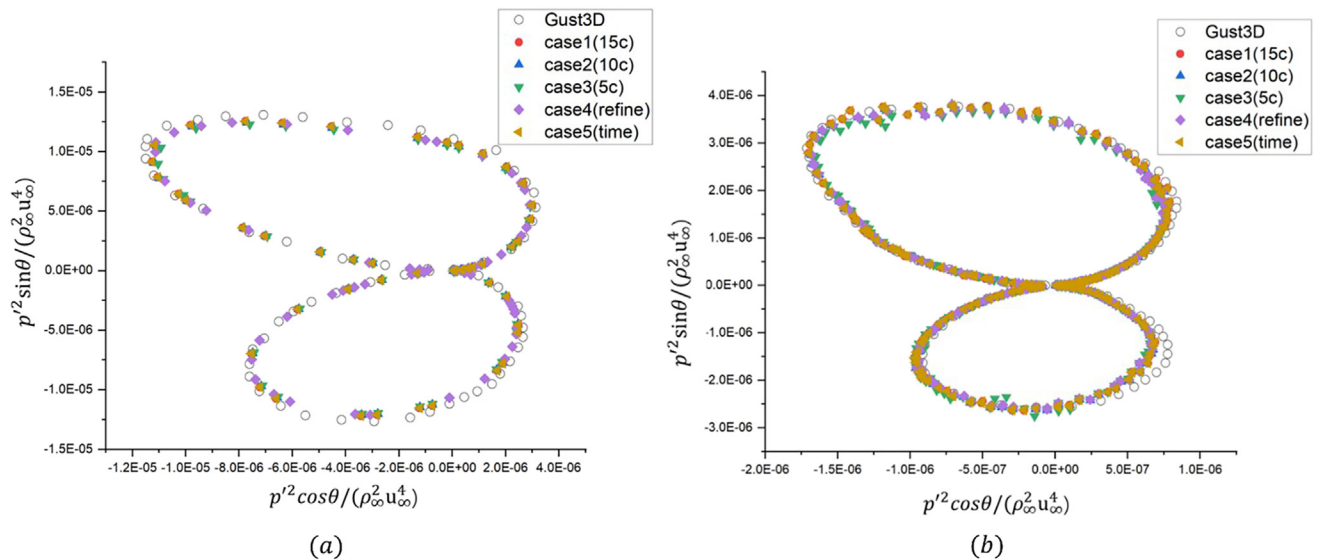

FIG. 3. Average squared sound pressure on two circles: (a) $R = 1c$ (one chord length) and (b) $R = 4c$ (four-chord length).

meshes is the best way to translate available resources into resolution power for spectral/hp element methods.[38] With the increase in the order of polynomials, the resolution can be improved faster than just increasing the mesh number with the same computation cost.

IV. THE SCALING LAWS OF MACH NUMBER

This section investigates the effect of Mach number on gust–airfoil interaction noise using the CAA method validated in Sec. III and the flat-plate theory, aiming to develop an efficient method to predict the sound pressure for airfoils at different Mach numbers without the time-consuming CAA process.

The numerical setup is the same as the validation part. The origin of the coordinate system is located at the leading edge of the airfoil. The reference values used here are defined as

$$L_{ref} = c; \quad u_{ref} = a_\infty, \quad \rho_{ref} = \rho_\infty; \quad p_{ref} = \rho_\infty a_\infty^2, \quad (11)$$

where a_∞ is the sound speed in the far-field.

A. The sound pressure generated by gust–airfoil interaction with different Mach numbers

The sound generated by the interaction of gust and NACA0012 airfoil with different mean-flow Mach numbers is simulated to study the effect of Mach number. The gust [defined in Eq. (4)] is the same for all cases. The wavelength of the gust is $1c$ ($k = 1$). The contours of sound pressure generated by the gust–airfoil interaction with different Mach numbers are presented in Fig. 4. It is found that the wavelength of the generated sound increases with the increase in Mach number. The wavelength of a generated sound can be calculated by

$$\lambda = \frac{2\pi u_s}{\omega} = \frac{2\pi u_s}{k_1 u_g}, \quad (12)$$

where λ is the wavelength of generated sound, u_s is the non-dimensional velocity of sound propagation, which is the superposition of sound speed and mean-flow velocity, u_g is the non-dimensional velocity of gust, k_1 is the gust wavenumber in the stream direction, ω
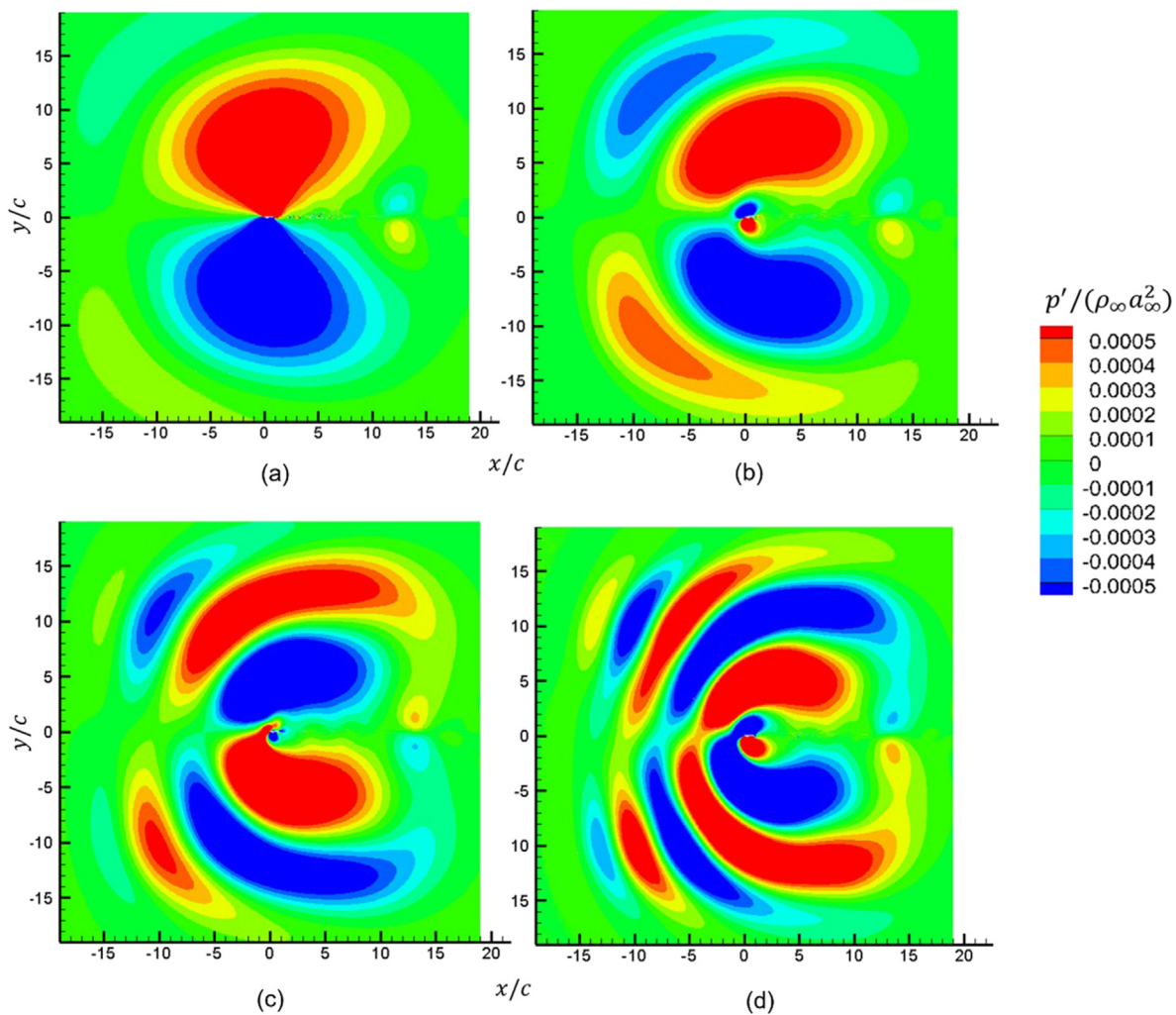

FIG. 4. Contours of sound pressure generated by gust–airfoil interaction with different Mach numbers: (a) $Ma = 0.2$; (b) $Ma = 0.3$; (c) $Ma = 0.4$; and (d) $Ma = 0.5$.
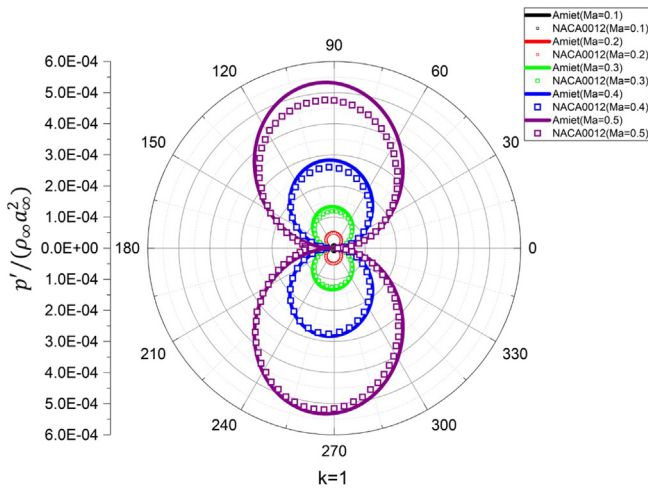
FIG. 5. Radiated sound pressure on the circle with $R = 4c$ for different Mach numbers ($Ma = 0.1 - 0.5$).

is the angular frequency of gust, which is the same as sound. So the generated sound wavelength in the upstream direction is smaller than the one in the downstream direction, especially for high Mach number cases.

The sound pressure of the NACA0012 airfoil on a circle with a radius of 4c is given by a polar diagram in Fig. 5. The results calculated by the flat-plate theory (named Amiet in Fig. 5) are provided for comparison. First, we consider a gust with low reduced frequency ($k = 1$). The sound pressure is found to increase with Mach number. When the Mach numbers are relatively small (Ma = 0.1–0.2), the sound

pressure calculated from the flat-plate theory agrees well with the CAA results. However, the flat-plate theory overpredicts the radiated pressure at high Mach numbers (Ma = 0.5). The same trend can be found for NACA0006 and NACA0002 airfoils. However, with the decrease in the airfoil thickness, the flat-plate theory gives better prediction even at high Mach numbers. We believe this is due to the airfoil thickness effect, which reduces radiated sound more significantly at high Mach numbers. The sound generated by the NACA0006 and NACA0012 airfoil is also studied. The results are not presented here.

B. The Mach number scaling law for gust–airfoil interaction noise

Singer *et al.*[44] studied the scaling law for the sound scattered by a trailing edge. They found the mean square pressure varies as $Ma^{5.2}$ and the exponent changes slightly with the observer angle. Here, we define a similar form of scaling law,

$$\frac{p_1}{p_2} = \left(\frac{Ma_1}{Ma_2}\right)^q, \tag{13}$$

where p_1 and p_2 are sound pressures in an observer from two Mach numbers Ma_1 and Ma_2, correspondingly.

Now the problem is to find the value q for gust–airfoil interaction. Variation of the squared sound pressure with Mach number is plotted in Fig. 6 for different observers. In our study, all observers were located in a circle with radius $R = 4c$ (c is the chord length of airfoils). The symbols stand for the sound pressure calculated by the flat-plate theory and the CAA method for corresponding Mach numbers. Here, the sound pressure calculated by the flat-plate theory and the CAA results of NACA0002, NACA0006, and NACA0012 airfoils are plotted in black, red, green, and blue, respectively. The lines represent the best-fit power-law of the Mach number, as given in Eq. (13).
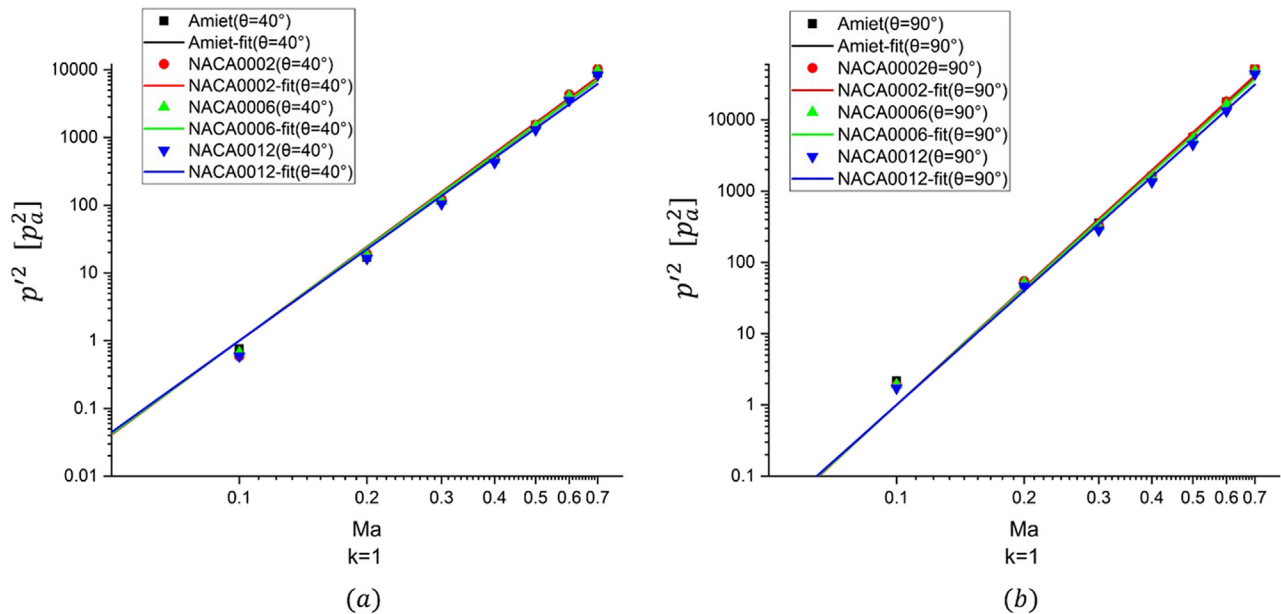

FIG. 6. Variation in the ratio of squared sound pressure vs the ratio of Mach number with $k = 1$. (a) $\theta = 40°$ and (b) $\theta = 90°$.

TABLE II. The value for the power of Mach numbers.

ϑ	The flat-plate theory		NACA0002		NACA0006		NACA0012	
	$k=1$	$k=8$	$k=1$	$k=8$	$k=1$	$k=8$	$k=1$	$k=8$
40°	4.796	5.068	4.998	4.98	4.888	4.95	4.882	4.842
90°	5.132	4.116	5.21	4.16	5.144	4.39	5.134	4.822

A good agreement can be obtained by the Amiet theory and the CAA results from NACA0002, NACA0006, and NACA0012. For an observer at 40°, the squared sound pressure varies as the 4.796 power of Mach number by the flat-plate theory. For an observer at 90°, the regression indicates variation with the 5.132 power of Mach number by the flat-plate theory. Table II lists all values for the power of Mach number by different results. The value varies for different observer angles, gust wavenumber, and thickness of airfoils. The sound pressure increases quicker at 90° than at 40° for all cases with different gust wavenumbers and different thicknesses.

Two observers in the upstream are chosen to the scaling law in upstream direction. Figures 7 and 8 give the squared sound pressure and its fit-line for the observer at 120° and 150° with $k=1$ and $k=8$. For cases with $k=1$, the fit-line agrees well with each other for NACA0002, NACA006, and NACA0012 airfoil for the observer at 120°. Some differences are observed for the observer at 150°. However, large discrepancies can be observed for the result predicted by the flat-plate theory. The slope of the fit-line of the plate theory is smaller than the other fit-lines. For cases with $k=8$, large discrepancies are observed at both 120° and 150°.

The magnitude of gusts ($\sqrt{u'^2 + v'^2}/U_\infty$) is presented in Fig. 9. It is obvious that the wavelength of gust decreases with the increase in

wavenumber. The wavefront of gusts is presented by black lines in zoomed-in views. The gust wavefront is cutoff by the airfoil and two "gust-circles" are generated successively for the case with $k=1$. More gust-circles are found for the case with $k=8$, which may indicate the strong interaction between gusts and airfoils. This finding supports that the variation is more complex for the case with $k=8$ in Fig. 10. These gust-circles generates successively when gusts move with a mean flow, which leads to pressure fluctuation on the airfoil surface. This process is the fluid mechanics mechanism of sound generation for gust–airfoil interaction.

Here, we use a Fourier series with four terms to fit the trendline for cases $k=1$. The trendline can be used to predict sound pressure from one observer to another. The Fourier series with four terms can be defined as

$$q(x) = a_0 + a_1\sin(wx) + b_1\sin(wx) + a_2\sin(2wx) + b_2\sin(2wx)$$
$$+ a_3\sin(3wx) + b_3\sin(3wx) + a_4\sin(4wx) + b_4\sin(4wx),$$
(14)

where q is the power of Mach number, and x is the observers' angles.

Figure 10 shows the relationship between values for the power of Mach numbers (corresponding to squared sound pressure) and angles of observers with $k=1$ and 8. Different symbols represent the power of Mach number by the flat-plate theory, NACA0002, NACA0006, and NACA0012 airfoil, respectively. Because the sound pressure is very small at 0° and 180°, there is a strong scattering of the power of Mach number at 0° and 180°. So the points near 0° and 180° are neglected to give a better fit. We find the Fourier series with four terms fits the variation well. The result from the Amiet theory agrees well with NACA0002. With the increase in thickness, the power of Mach number increases from about 3.75 to 4.3 near 180°. The maximum value decreases near 90° and 270°, and the respective angle shifts
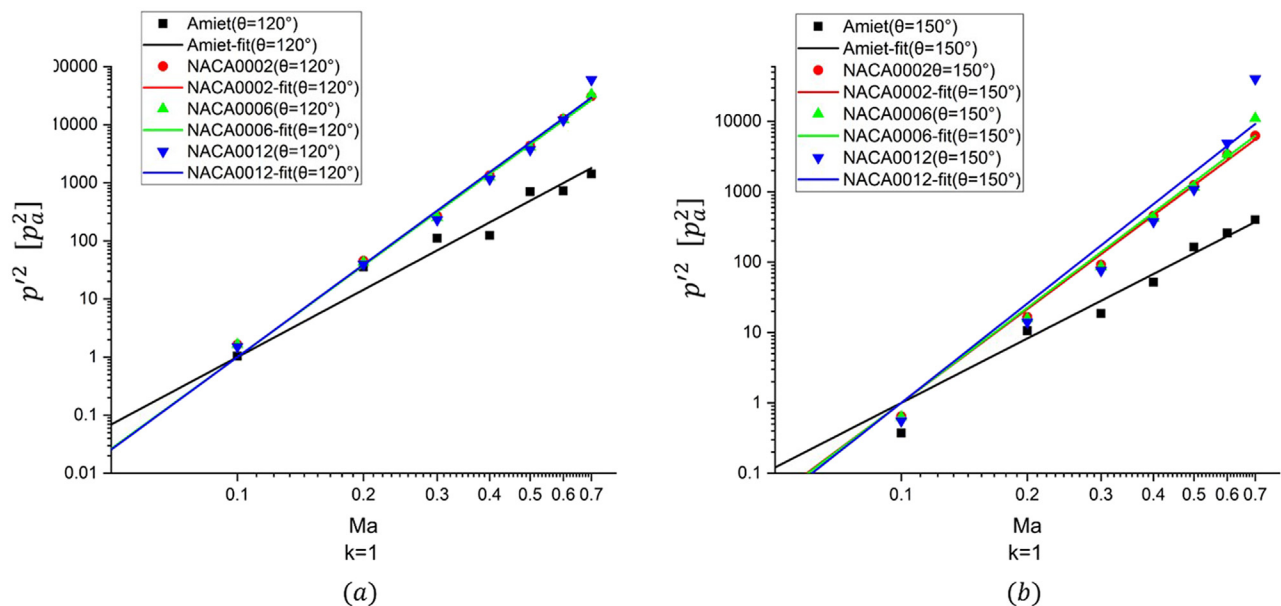
FIG. 7. Variation in the ratio of squared sound pressure vs the ratio of Mach number with $k=1$. (a) $\theta = 120°$ and (b) $\theta = 150°$.
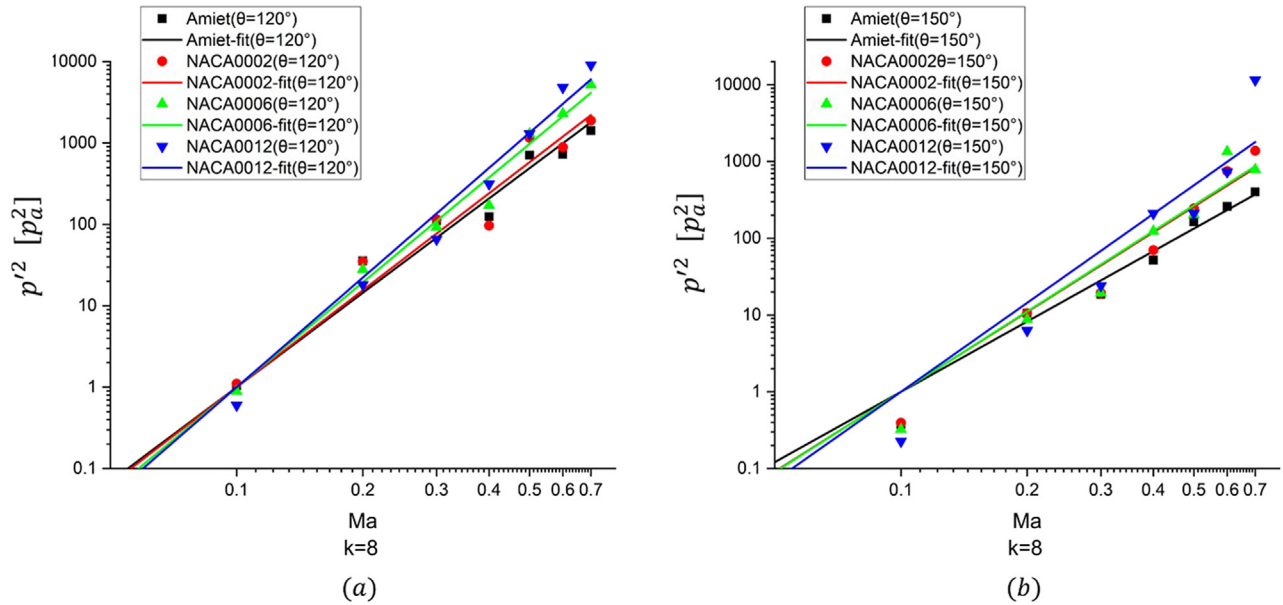
FIG. 8. Variation in the ratio of squared sound pressure vs the ratio of Mach number with $k = 8$. (a) $\theta = 120°$ and (b) $\theta = 150°$.
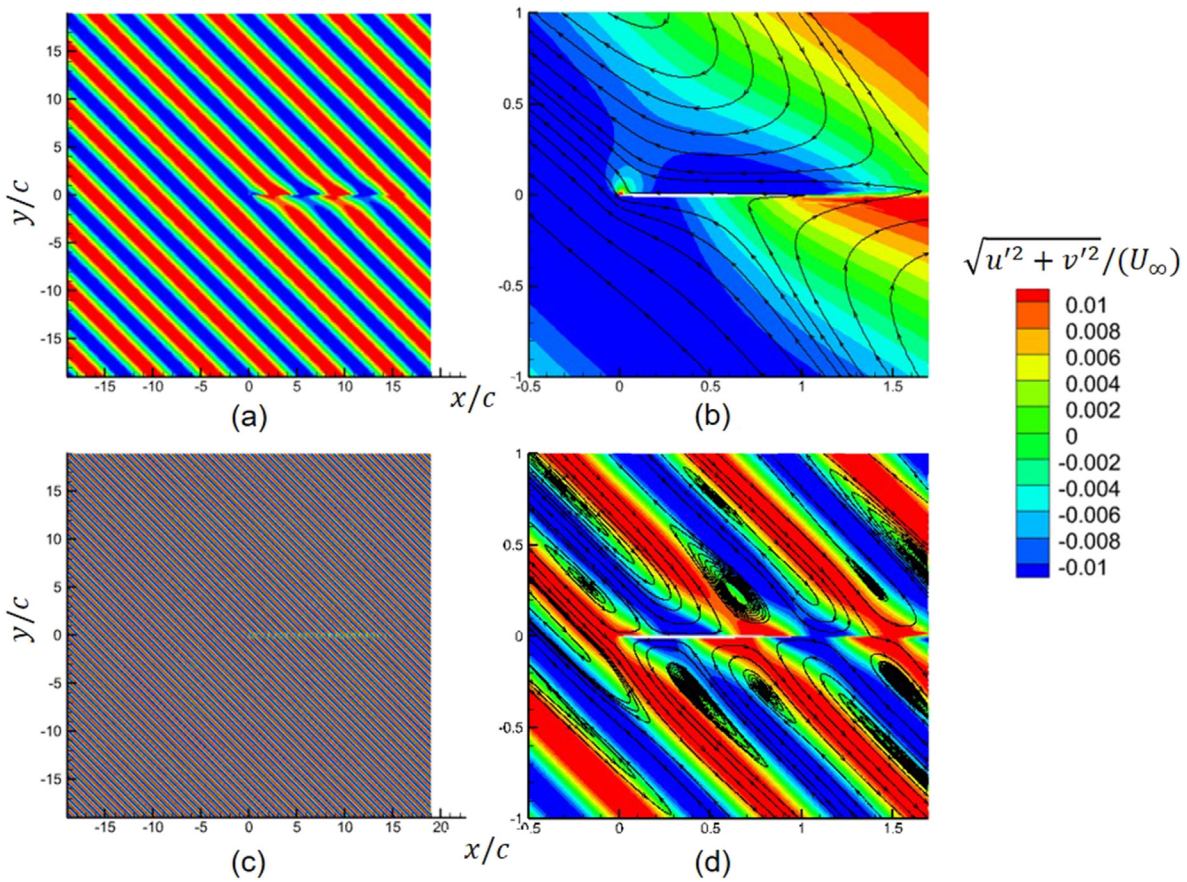

FIG. 9. Contours of gust magnitude and zoomed-in view near the NACA0002 airfoil: (a) $k = 1$; (b) $k = 1$ zoomed-in view; (c) $k = 8$; and (d) $k = 8$ zoomed-in view.
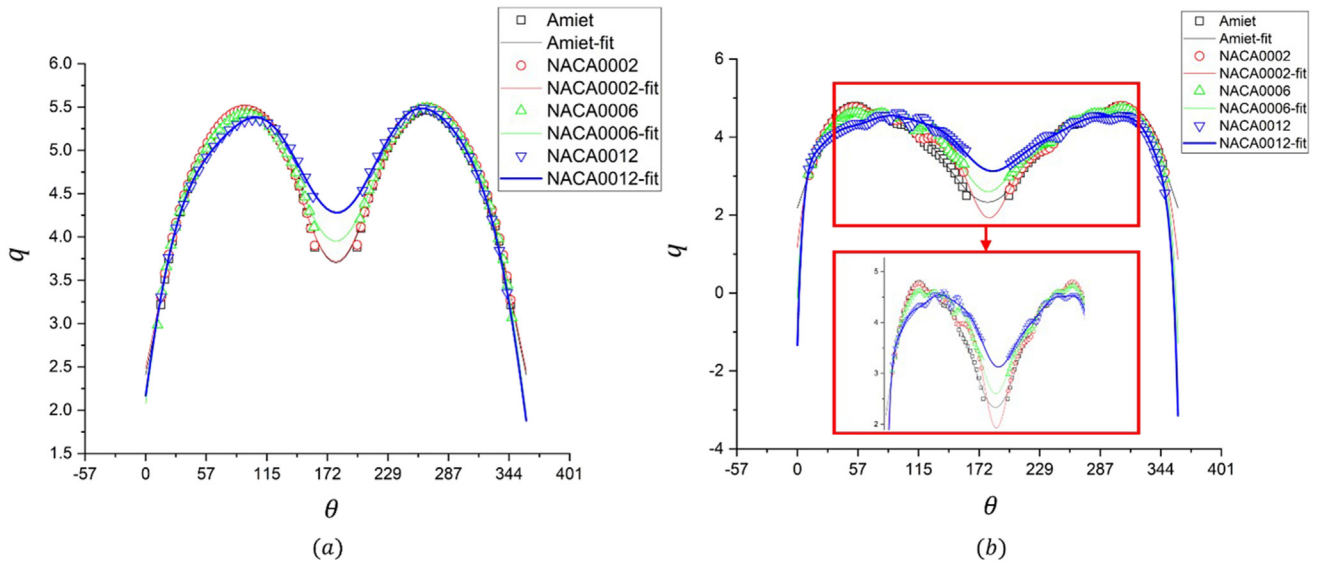
FIG. 10. Variation in the power of Mach number vs angles of observers: (a) $k = 1$ and (b) $k = 8$.

slightly. So we can find the sound pressure increases quicker at 90° and 270° with the maximum power of Mach number, and the sound pressure for the thicker airfoil increases slower at 90° and 270°.

For the case with $k = 8$. The Fourier series with eight terms has to be used to fit the trendline. The trendline is much more complicated than the one with $k = 1$. Even though a Fourier series with eight terms is used, the variation at 90° and 270° cannot be captured. The variation at 90° and 270° may indicate new lobes generated. In addition, the result from the Amiet theory is different from NACA0002. This means that with a bigger gust wavenumber, the thickness effect is more important than the case with a smaller gust wavenumber. This may be due to the complex interaction of sound sources on the airfoil surface.

V. PREDICTING SOUND PRESSURE WITH THE SCALING LAW

In this section, the sound pressure at the circle with $R = 4c$ is calculated from data at other Mach numbers to $Ma = 0.5$ by the scaling laws given in Sec. IV. For the cases with $k = 1$, a Fourier series with four terms are used. For the cases with k = 8, a Fourier series with eight terms is used. The scaling laws are obtained from both CAA results and the flat-plate theory (represented by "Amiet" in figures presented later).

A. Predicting sound pressure with $k = 1$

Figure 11(a) shows the scaled sound pressure by scaling laws compared with the CAA results at $Ma = 0.5$ for airfoils with NACA0002 airfoil. The circle stands for the CAA results. The solid lines show the scaled sound pressure by the scaling law from the flat-plate theory. The dotted lines present the scaled sound pressure by the scaling law from the CAA results. We find that the difference in the scaled sound pressure between the flat-plate theory and CAA results is negligible for the NACA0002 airfoil. The scaled sound pressure from Mach numbers 0.3 to 0.6 gives a better fit than from Mach numbers

0.1, 0.2, and 0.7. This is reasonable because these Mach numbers 0.1, 0.2, and 0.7 are far away from the base Mach number 0.5.

Figures 11(b) and 11(c) present the scaled sound pressure for NACA0006 and NACA0012 airfoil with $k = 1$. With the increase in airfoil thickness, the difference of the scaled sound pressure between the flat-plate theory and CAA results increases, especially for NACA0012 airfoil of Mach numbers 0.1, 0.2, and 0.7. This is caused by the fact that the sound pressure decreases with the increase in airfoil thickness. For NACA0006 and NACA0012 airfoils, the scaled sound pressure by the scaling law from CAA results fit better than the flat-plate theory. In addition, the scaled sound pressure from the NACA0012 airfoil overpredicts the sound pressure in the upstream direction. This situation does not exist in the case of the NACA0002 airfoil. It is believed the airfoil thickness plays another role in the high Mach number range, like $Ma = 0.7$. A further research will be performed in the future.

B. Predicting sound pressure with $k = 8$

The scaled sound pressure for the cases of $k = 8$ is not predicted as well as $k = 1$ due to lobes in the directivity. Figures 12(a)–12(c) show the scaled sound pressure for NACA0002, NACA0006, and NACA0012 airfoil with $k = 8$. The difference of the scaled sound pressure between the flat-plate theory and CAA results increases with the increase in airfoil thickness, which is the same as the cases with $k = 1$. The scaled sound pressure from $Ma = 0.1, 0.2, 0.3$ cannot capture the new lobe generated at 120° in the case with Mach number 0.5. More lobes are still found for the scaled sound pressure from $Ma = 0.6, 0.7$. This means that the scaling law cannot capture lobe generation. Attention should be paid when the scaling laws are used for the high reduced frequency cases because new lobes will be generated. In addition, the scaled sound pressure in the upstream direction is still overpredicted for the case with NACA0012 airfoil at $Ma = 0.7$.
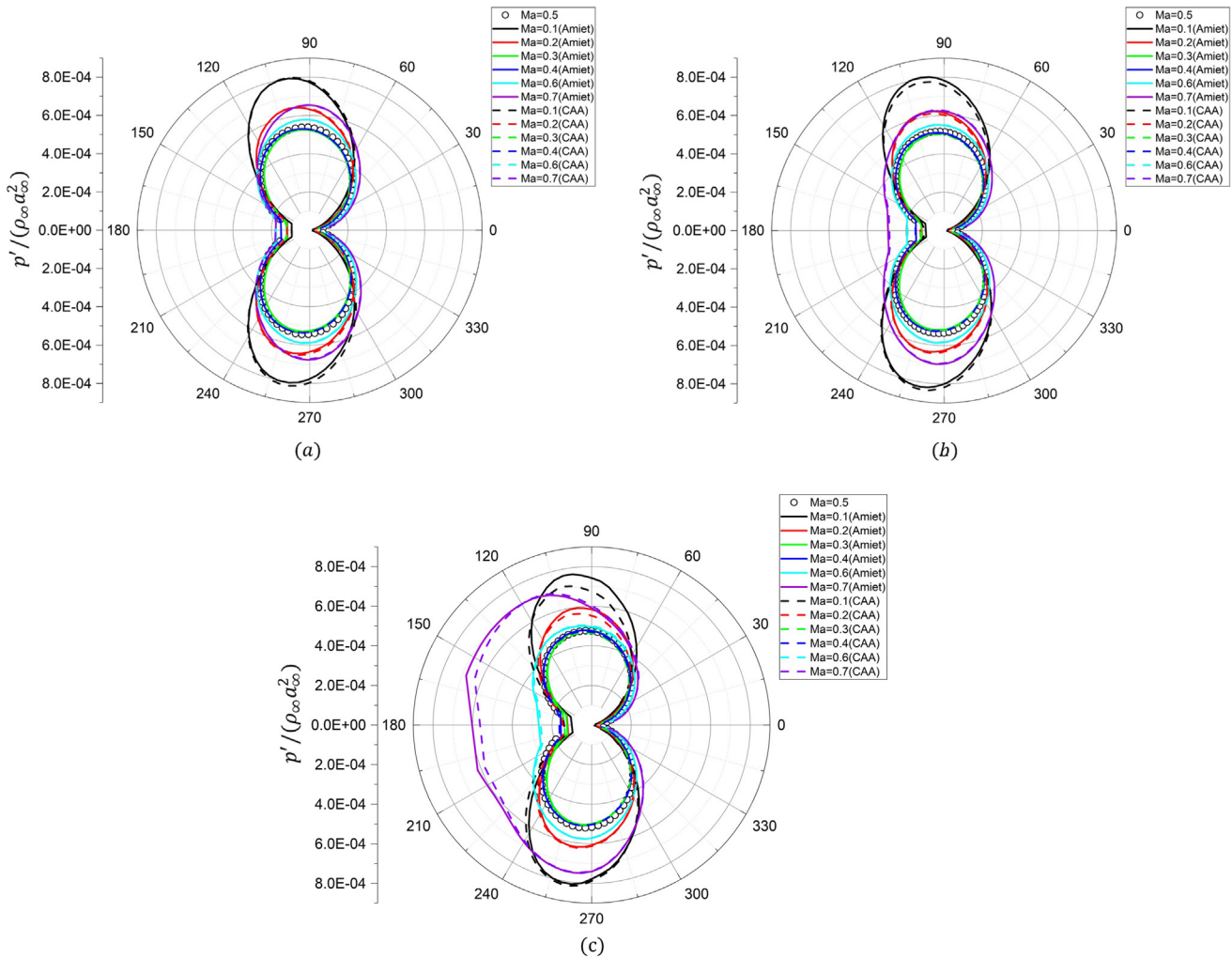
FIG. 11. Sound pressure at $Ma = 0.5$ from direct CAA simulation and the scaled sound pressure by scaling laws from both CAA and the flat-plate theory results ($k = 1$): (a) NACA0002 airfoil; (b) NACA0006 airfoil; and (c) NACA0012 airfoil.

This situation is found in both $k = 1$ and $k = 8$, which means the situation may be independent of the gust wavenumber.

It is worth mentioning that high Ma flow can be regarded as high-frequency cases, which retain the directivity of high k values (e.g., $k = 8$). In some sense, the Mach number is related to the Helmholtz number. So it is more easy to predict the sound pressure with similar directivity. Figure 13 presents the sound pressure given by two cases with $k = 4\,Ma = 0.7$ and $k = 8\,Ma = 0.5$. Similar sound directivity pattern can be found for these two cases, which supports the idea above.

VI. PREDICTING SOUND PRESSURE WITH THE FLAT-PLATE THEORY

A large discrepancy is found for the scaled sound pressure for the case at Mach numbers 0.1, 0.2, and 0.7. In this section, the sound pressure is predicted by using the CAA results as the base sound pressure

and the ratio of sound pressure calculated from the flat-plate theory as shown by the following equation:

$$p'_{ob} = p'_{ba}\left(\frac{p'_{ob-Amiet}}{p'_{ba-Amiet}}\right), \qquad (15)$$

where p'_{ob} is the objective sound pressure, and p'_{ba} is the base sound pressure from CAA simulation. $p'_{ob-Amiet}$ is the sound pressure calculated by the flat-plate theory using the same Mach number with p'_{ob}. $p'_{ba-Amiet}$ is the sound pressure calculated by the flat-plate theory using the same Mach number with p'_{ba}.

A. Predicting sound pressure to $Ma = 0.5$ for $k = 1$

Figure 14 presents the scaled sound pressure from Eq. (15) for the NACA0012 airfoil with $k = 1$. The circles stand for the results of the CAA method. The dashed line represents the results of the flat-
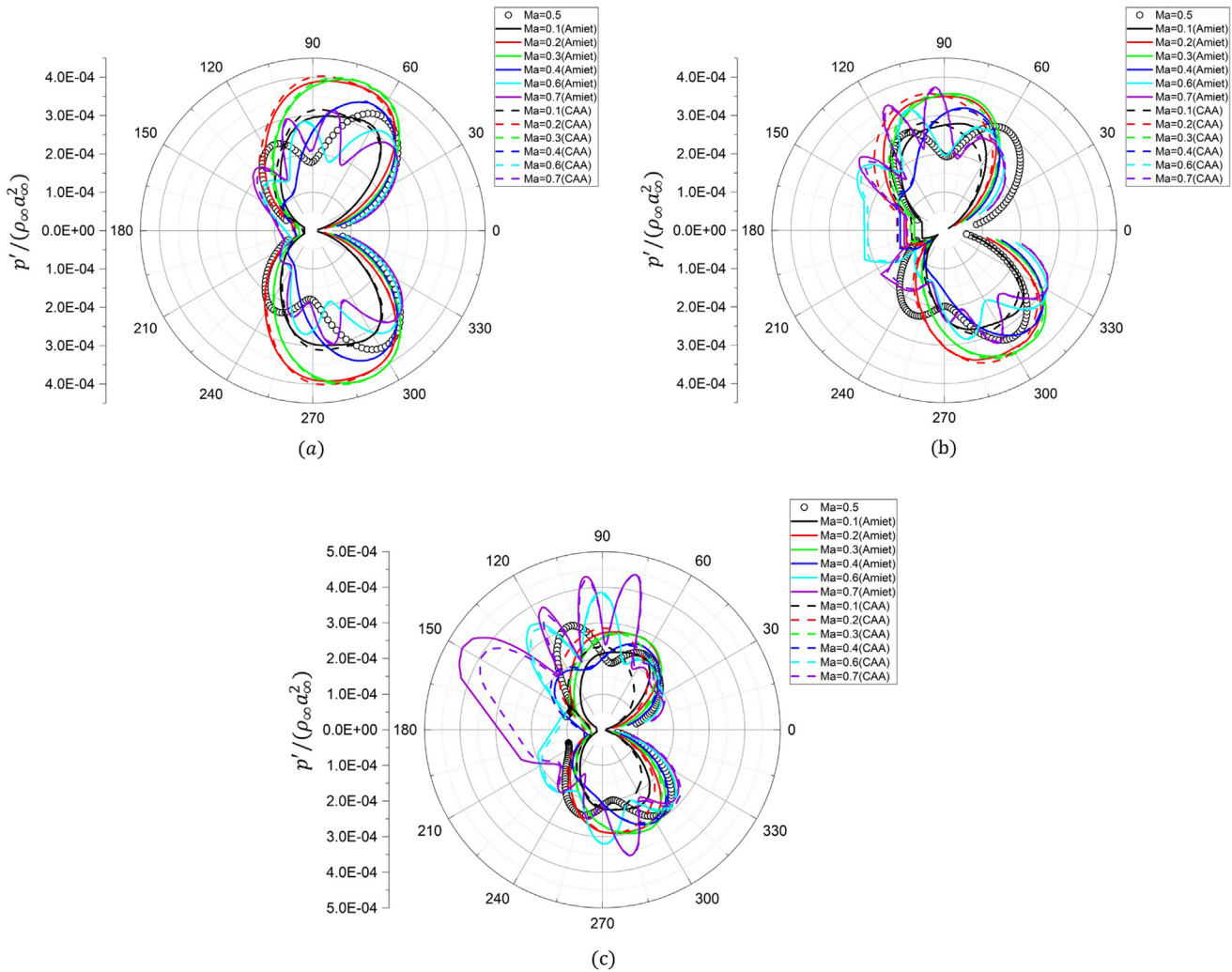
FIG. 12. Sound pressure at $Ma = 0.5$ from direct CAA simulation and the scaled sound pressure by scaling laws from both CAA and the flat-plate theory results ($k = 8$): (a) NACA0002; (b) NACA0006; and (c) NACA0012.

plate theory. The color of different lines shows the results by the scaling law for other Mach numbers. All the sound pressure generated by other Mach numbers is scaled to the sound pressure with Ma = 0.5. We find all the sound pressures obtained by Eq. (15) agree better with the CAA results than the result directly from the flat-plate theory. In other words, we can use other Mach numbers (like Ma = 0.1–0.4) and Eq. (15) to calculate the sound pressure at Ma = 0.5. This method will get a better result than the one directly calculated by the flat-plate theory.

Figure 14 shows the scaled sound pressure for the NACA0006 airfoil with $k = 1$. We find all the methods agree well with each other. Even Amie's theory can give a good prediction. The sound reduction due to the thickness is slight. So we think Amie's theory can be used for the airfoil with a thickness smaller than NACA0006 airfoil (just for symmetry airfoil with zero angle of attack).

B. Predicting sound pressure to $Ma = 0.2$ for $k = 1$

The above case scales sound pressure to Ma = 0.5 from lower Mach numbers. Here, we try to scale high Mach numbers to a small Mach number. Figure 15(a) presents the scaled sound pressure for $Ma = 0.2$ with $k = 1$. We find the flat-plate theory gives a better result for the case $Ma = 0.2$. The reason may be related to the wavelength of generated sound in $Ma = 0.2$, which is much bigger than the chord length of the airfoil. So the effect of thickness is insignificant.

The scaled sound pressure of the NACA0006 airfoil is presented in Fig. 15(b). The sound pressure agrees well with each other except for a bit of underprediction compared to CAA results. The flat-plate theory still performs well in giving a good prediction. These studies indicate that the flat-plate theory performs well for small thickness cases or low Mach numbers. However, for a thicker airfoil in high Mach number (like $Ma = 0.5$), the scaled sound pressure from Eq. (15) can give better results.
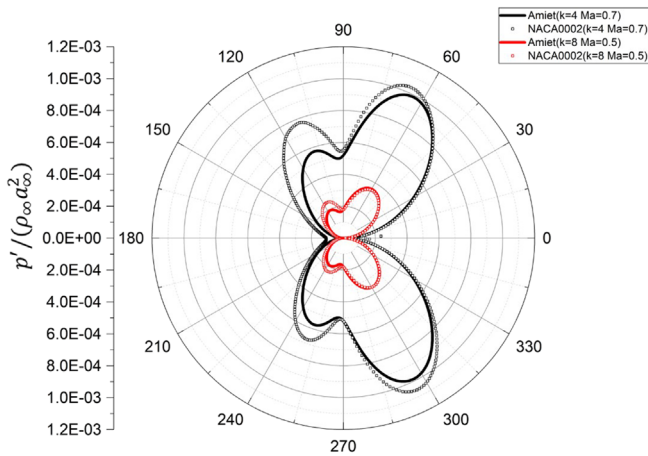
FIG. 13. Sound pressure given by two cases with $k = 4$ $Ma = 0.7$ and $k = 8$ $Ma = 0.5$.

C. Predicting sound pressure to $Ma = 0.5$ for $k = 8$

For low reduced frequency gusts, the sound directivity has a dipole-like pattern. Equation (15) works well for the cases with $Ma = 0.1$–0.5. However, new lobes are generated in the sound directivity for high reduced frequency gusts. It is more challenging to predict the sound pressure for these cases. Figure 16(a) presents the scaled sound pressure by NACA0012 with $k = 8$. The flat-plate theory overpredicts the sound pressure at $60°$ and underpredicts it at $105°$. The scaled sound pressure given by Eq. (12) can give a better result at $60°$. However, the sound pressure at $105°$ is still underpredicted. The scaled sound pressure from $Ma = 0.4$ has almost the same peak amplitude for the upstream lobe with $Ma = 0.5$. However, the angle of peaks is different.

The scaled sound pressure of NACA0006 is also presented in Fig. 16(b). The flat-plate theory underpredicts at $105°$ and overpredicts at

$60°$. In addition, the scaled sound pressure can give a better result at $60°$ than the flat-plate theory. However, both the flat-plate theory and Eq. (13) underpredict the sound pressure at $105°$. The flat-plate theory and Eq. (15) perform better for the NACA0006 airfoil than for the NACA0012 airfoil. This may be due to the effect of airfoil thickness. Figure 16(c) shows the scaled sound pressure for the NACA0002 airfoil. The sound pressure predicted by the flat-plate theory agrees well with the CAA simulation at $60°$. The sound pressure at $105°$ is still underpredicted by both the flat-plate theory and Eq. (15). In this case, the flat-plate theory can give a better result. So, the CAA simulation is not needed for the NACA0002 airfoil. For the airfoil thickness smaller than NACA0006, the discrepancy between the flat-plate theory and Eq. (15) is small. So, Eq. (15) is suitable for predicting the sound pressure given by thicker airfoils.

D. Predicting sound pressure to $Ma = 0.2$ for $k = 8$

The sound pressure scaled from a higher Mach number is also studied here. Figure 17(a) presents the sound pressure for the NACA0012 airfoil scaled to $Ma = 0.2$. Only the sound pressure scaled from $Ma = 0.2$, 0.3 agrees well with CAA results. The flat-plate theory overpredicts the sound pressure due to the thickness of the NACA0012 airfoil. The sound pressure scaled from $Ma = 0.4$, 0.5 is overpredicted upstream. This may occur due to other lobes in the upstream direction at a higher reduced frequency. The reason for this phenomenon is the underprediction of Amiet's theory in upstream lobes. So, from a low Mach number scaled to a high Mach number, the sound pressure is underpredicted upstream. On the contrary, the sound pressure is scaled from a higher Mach number, and the sound pressure is overpredicted upstream.

The conclusion is verified again for the sound pressure of NACA0006, as shown in Fig. 17(b). The sound pressure of $Ma = 0.1$, 0.3 agrees well with the CAA results. The solution of the flat-plate theory is slightly overpredicted. The sound reduction is minor for the NACA0006 airfoil compared with the NACA0012 airfoil. The
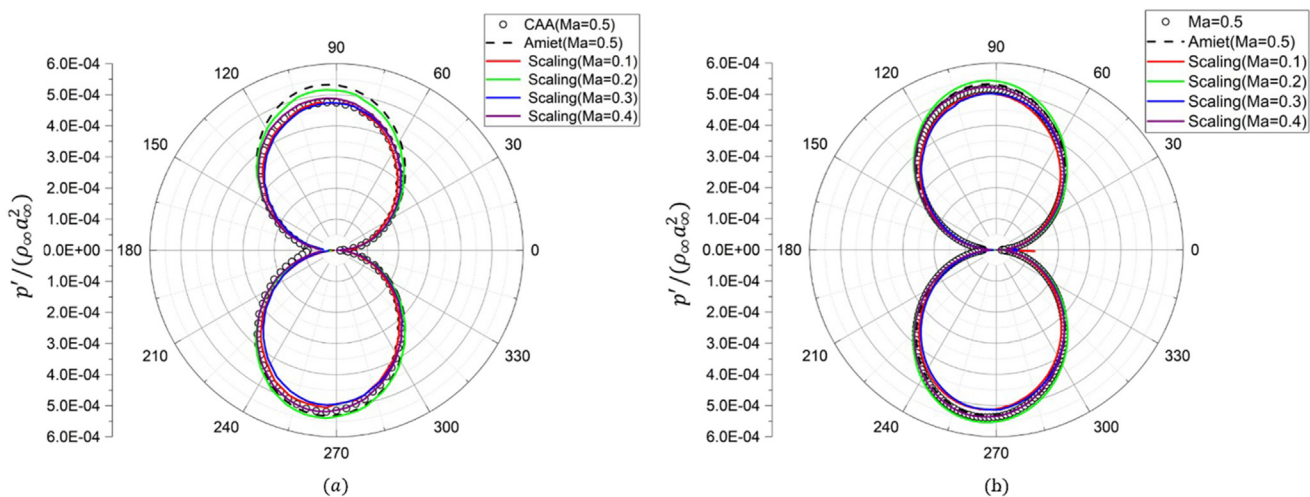
FIG. 14. Sound pressure at $Ma = 0.5$ from direct CAA simulation. The flat-plate theory and scaled from other Mach number CAA results to $Ma = 0.5$ ($k = 1$): (a) NACA0012 and (b) NACA0006.
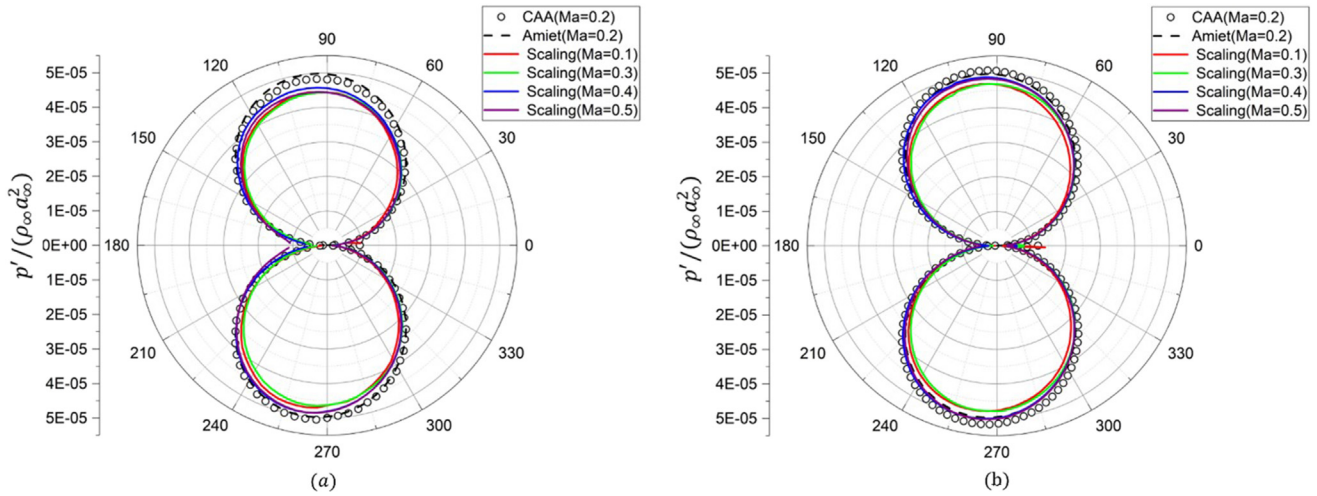
FIG. 15. Sound pressure at $Ma = 0.2$ from direct CAA simulation, the flat-plate theory, and scaled from other Mach number CAA results to $Ma = 0.2$ ($k = 1$): (a) NACA0012 and (b) NACA0006.
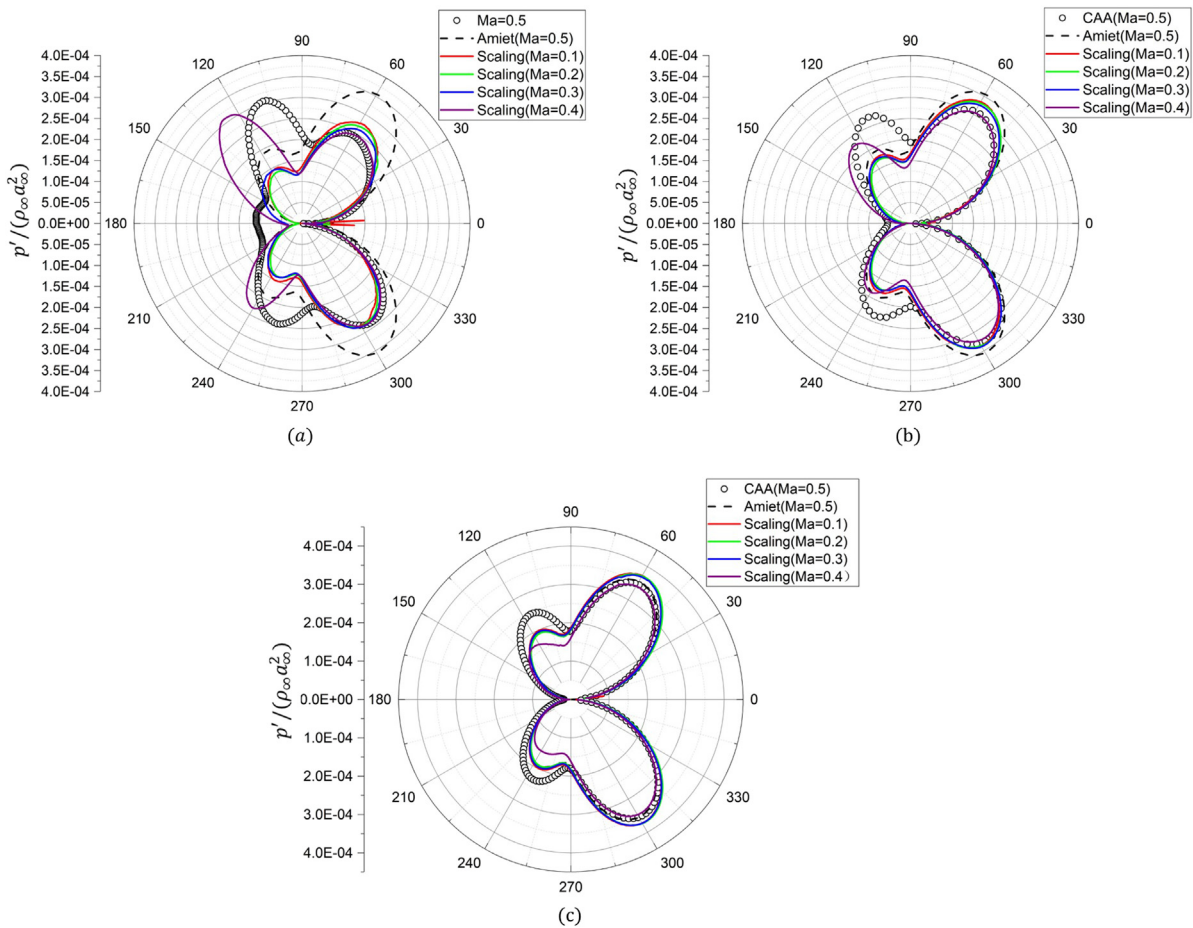

FIG. 16. Sound pressure at $Ma = 0.5$ from direct CAA simulation, the flat-plate theory, and scaled from other Mach number CAA results to $Ma = 0.5$ ($k = 8$): (a) NACA0012; (b) NACA0006; and (c) NACA0002.
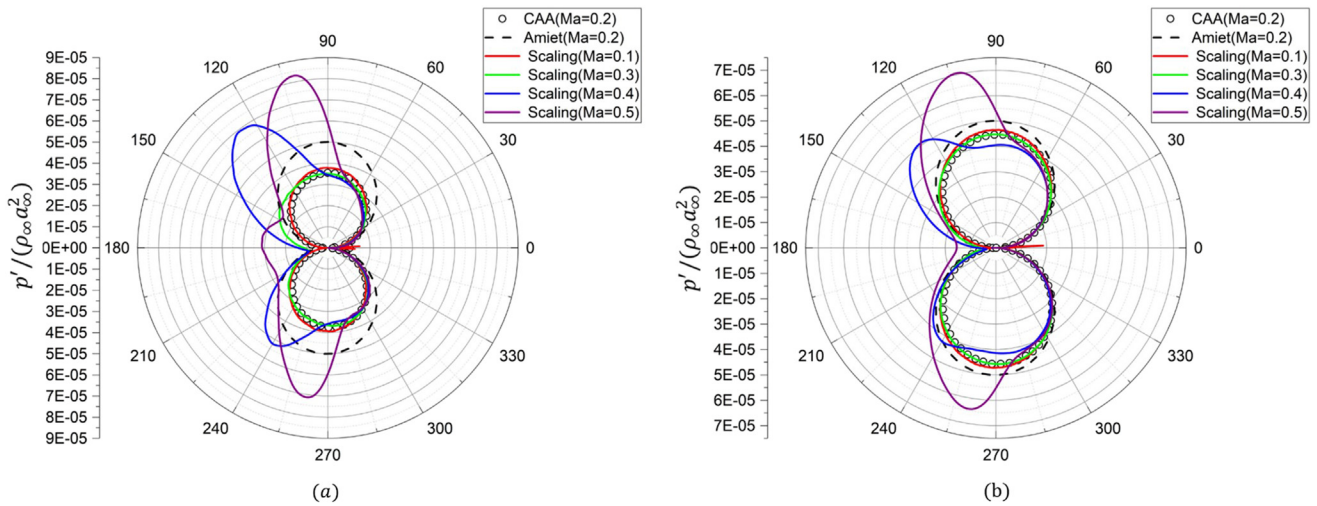
FIG. 17. Sound pressure by the CAA method, the flat-plate theory, and scaling law for other Mach numbers scaled to Ma = 0.2 ($k = 8$): (a) NACA0012 and (b) NACA0006.

sound pressure scaled from $Ma = 0.4$, 0.5 is overpredicted upstream. We can notice that thickness plays a vital role in sound reduction.

VII. SUMMARY

The scaling law of the sound generated by gust–airfoil interaction is studied using results from the flat-plate theory and CAA simulation. For airfoil thickness smaller than NACA0006 airfoil, the difference is negligible for the scaled sound pressure for these methods. For NACA0012, a considerable difference can be found. The scaled sound pressure by using the scaling law from CAA results fit better.

The squared sound pressure varies with the Mach number as the power of 5.132 at $\theta = 90°$ by the flat-plate theory with $k = 1$. The power of the Mach number changes with the angles of observers. In our study, Fourier series with four terms are used to fit the power of Mach number vs angles of observers for $k = 1$.

Another way to scale the sound pressure for different Mach numbers is given by using the CAA results as the base sound pressure and the ratio of sound pressure calculated from the flat-plate theory as shown by Eq. (15). This method improves the prediction compared with scaling laws by the flat-plate theory and CAA results. It gives a better result than the flat-plate theory for the airfoil with a thickness larger than the NACA0006 airfoil. For high reduced frequency cases, the sound pressure upstream is difficult to predict because the sound pressure, calculated by the flat-plate theory, is underpredicted upstream.

To give a guide for sound prediction, in a high Mach number range ($Ma \geq 0.5$), when the thickness of the airfoil is larger than NACA0006, the scaled sound pressure can give a better prediction for low reduced frequency cases and the downstream directions for high reduced frequency cases. Otherwise, the flat-plate theory can predict the sound generated by low reduced frequency gust–airfoil interaction.

ACKNOWLEDGMENTS

AUTHOR DECLARATIONS
Conflict of Interest

The authors have no conflicts to disclose.

Author Contributions

Shujie Jiang: Conceptualization (equal); Data curation (equal); Formal analysis (equal); Investigation (equal); Validation (equal); Visualization (equal); Writing – original draft (equal). **Yanan Wang:** Writing – review & editing (equal). **Zhenguo Yan:** Methodology (equal). **Rongping Zhang:** Writing – review & editing (equal). **Zhiwei Hu:** Conceptualization (equal); Supervision (equal); Writing – review & editing (equal).

DATA AVAILABILITY

The data that support the findings of this study are available from the corresponding author upon reasonable request.

REFERENCES

[1]N. J. Wei, J. Kissing, T. Wester, S. Wegt, and C. Tropea, "Insights into the periodic gust response of airfoils," J. Fluid Mech. **876**, 237 (2019).

[2]J. T. Bonet, H. G. Schellenger, B. K. Rawdon, K. R. Elmer, S. R. Wakayama, D. L. Brown, and Y. Guo, "Environmentally responsible aviation (ERA) project-N + 2 advanced vehicle concepts study and conceptual design of subscale test vehicle (STV) Final Report," Report No. NASA/CR-2011-216519, 2011.

[3]K. S. Brentner and F. Farassat, "Modeling aerodynamically generated sound of helicopter rotors," Prog. Aerosp. Sci. **39**(2–3), 83 (2003).

[4]U. W. Ganz, P. D. Joppa, T. J. Patten, and D. F. Scharpf, "Boeing 18-inch fan rig broadband noise test," Report No. NASA/CR-1998-208704, 1998.

[5]V. P. Blandeau and P. F. Joseph, "Broadband noise due to rotor-wake/rotor interaction in contra-rotating open rotors," AIAA J. **48**(11), 2674 (2010).

[6]V. Blandeau, P. Joseph, and B. Tester, "Broadband noise prediction from rotor-wake interaction in contra-rotating propfans," AIAA Paper No. 2009-3137, 2009, p. 3137.

[7]M. Kingan, V. Blandeau, B. Tester, P. Joseph, and A. Parry, "Relative importance of open rotor tone and broadband noise sources," AIAA Paper No. 2011-2763, 2011, p. 2763.

[8]F. Gea-Aguilera, X. Zhang, X. Chen, J. R. Gill, and T. Nodé-Langlois, "Synthetic turbulence methods for leading edge noise predictions," AIAA Paper No. 2015-274, 2015, p. 274.

[9]L. J. Ayton and P. Chaitanya, "Analytical and experimental investigation into the effects of leading-edge radius on gust-aerofoil interaction noise," J. Fluid Mech. **829**, 780 (2017).

[10]L. J. Ayton and N. Peake, "On high-frequency sound generated by gust-aerofoil interaction in shear flow," J. Fluid Mech. **766**, 297 (2015).

[11]I. Evers and N. Peake, "Noise generation by high-frequency gusts interacting with an airfoil in transonic flow," J. Fluid Mech. **411**, 91 (2000).

[12]X.-Y. Wang, A. Himansu, S.-C. Chang, and P. C. E. Jorgenson, "Computation of a single airfoil gust response and gust-cascade interaction using the CE/SE method," in Proceedings of the Fourth Computational Aeroacoustics (CAA) Workshop on Benchmark Problems (2004).

[13]J. Gill, X. Zhang, and P. Joseph, "Symmetric airfoil geometry effects on leading edge noise," J. Acoust. Soc. Am. **134**(4), 2669 (2013).

[14]W. R. Sears, "Some aspects of non-stationary airfoil theory and its practical application," J. Aeronaut. Sci. **8**(3), 104 (1941).

[15]R. K. Amiet, "Acoustic radiation from an airfoil in a turbulent stream," J. Sound Vib. **41**(4), 407 (1975).

[16]R. Paterson and R. Amiet, "Acoustic radiation and surface pressure characteristics of an airfoil due to incident turbulence," AIAA Paper No. 1976-571, 1976, p. 571.

[17]H. M. Atassi, M. Dusey, and C. M. Davis, "Acoustic radiation from a thin airfoil in nonuniform subsonic flows," AIAA J. **31**(1), 12 (1990).

[18]R. W. Paterson and R. K. Amiet, "Noise and surface pressure response of an airfoil to incident turbulence," J. Aircr. **14**(8), 729 (1977).

[19]W. J. Devenport, J. K. Staubs, and S. A. L. Glegg, "Sound radiation from real airfoils in turbulence," J. Sound Vib. **329**(17), 3470 (2010).

[20]S. Zhong, X. Zhang, B. Peng, and X. Huang, "An analytical correction to Amiet's solution of airfoil leading-edge noise in non-uniform mean flows," J. Fluid Mech. **882**, A29 (2020).

[21]X. Huang, "A theoretical study of serrated leading edges in aerofoil and vortical gust interaction noise," Adv. Aerodyn. **1**(1), 6 (2019).

[22]A. Celik, L. Bowen, and M. Azarpeyvand, "Experimental investigation on the unsteady surface pressure fluctuation patterns over an airfoil," Phys. Fluids **34**(10), 105134 (2022).

[23]Y. Yang, M. Li, C. Ma, and S. Li, "Experimental investigation on the unsteady lift of an airfoil in a sinusoidal streamwise gust," Phys. Fluids **29**(5), 051703 (2017).

[24]T. Wang and L.-H. Feng, "Characterization of vertical and longitudinal gusts generated by twin pitching airfoils," Phys. Fluids **34**(9), 097116 (2022).

[25]Z. Wu, G. Bangga, T. Lutz, G. Kampers, and M. Hölling, "Insights into airfoil response to sinusoidal gusty inflow by oscillating vanes," Phys. Fluids **32**(12), 125107 (2020).

[26]N. Poudel, M. Yu, and J. T. Hrynuk, "Gust mitigation with an oscillating airfoil at low Reynolds number," Phys. Fluids **33**(10), 101905 (2021).

[27]J.-H. Seo, K. Menon, and R. Mittal, "A method for partitioning the sources of aerodynamic loading noise in vortex dominated flows," Phys. Fluids **34**(5), 053607 (2022).

[28]S. Narayanan, P. Chaitanya, S. Haeri, P. Joseph, J.-W. Kim, and C. Polacsek, "Airfoil noise reductions through leading edge serrations," Phys. Fluids **27**(2), 025109 (2015).

[29]H. Tian and B. Lyu, "Prediction of broadband noise from rotating blade elements with serrated trailing edges," Phys. Fluids **34**(8), 085109 (2022).

[30]S. Glegg and W. Devenport, *Aeroacoustics of Low Mach Number Flows: Fundamentals, Analysis, and Measurement* (Academic Press, 2017).

[31]B. A. Singer, K. S. Brentner, D. P. Lockard, and G. M. Lilley, "Simulation of acoustic scattering from a trailing edge," J. Sound Vib. **230**(3), 541 (2000).

[32]H. Xu, C. D. Cantwell, C. Monteserin, C. Eskilsson, A. P. Engsig-Karup, and S. J. Sherwin, "Spectral/*hp* element methods: Recent developments, applications, and perspectives," J. Hydrodyn. **30**(1), 1 (2018).

[33]M. D. Dahl, "Fourth computational aeroacoustics (CAA) workshop on benchmark problems," Report No. NASA/CP-2004-212954, 2004.

[34]G. Karniadakis and S. Sherwin, *Spectral/hp Element Methods for Computational Fluid Dynamics* (Oxford University Press, 2013).

[35]P. E. J. Vos, C. Eskilsson, A. Bolis, S. Chun, R. M. Kirby, and S. J. Sherwin, "A generic framework for time-stepping partial differential equations (PDEs): General linear methods, object-oriented implementation and application to fluid problems," Int. J. Comput. Fluid Dyn. **25**(3), 107 (2011).

[36]C. D. Cantwell, D. Moxey, A. Comerford, A. Bolis, G. Rocco, G. Mengaldo, D. de Grazia, S. Yakovlev, J.-E. Lombard, D. Ekelschot, B. Jordi, H. Xu, Y. Mohamied, C. Eskilsson, B. Nelson, P. Vos, C. Biotto, R. M. Kirby, and S. J. Sherwin, "Nektar++: An open-source spectral/*hp* element framework," Comput. Phys. Commun. **192**, 205 (2015).

[37]H. Xu, C. D. Cantwell, C. Monteserin, C. Eskilsson, A. P. Engsig-Karup, and S. J. Sherwin, "Spectral/*hp* element methods: Recent developments, applications, and perspectives," J. Hydrodyn. **30**(1), 1 (2018).

[38]R. C. Moura, S. J. Sherwin, and J. Peiró, "Linear dispersion–diffusion analysis and its application to under-resolved turbulence simulations using discontinuous Galerkin spectral/*hp* methods," J. Comput. Phys. **298**, 695 (2015).

[39]J. W. Kim, A. Lau, and N. D. Sandham, "Proposed boundary conditions for gust-airfoil interaction noise," AIAA J. **48**(11), 2705 (2010).

[40]A. Johnen, J.-F. Remacle, and C. Geuzaine, "Geometrical validity of curvilinear finite elements," J. Comput. Phys. **233**, 359 (2013).

[41]Z. G. Yan, Y. Pan, G. Castiglioni, K. Hillewaert, and S. J. Sherwin, "Nektar++: Design and implementation of an implicit, spectral/*hp* element, compressible flow solver using a Jacobian-free Newton Krylov approach," Comput. Math. Appl. **81**, 351 (2020).

[42]X.-Y. Wang, A. Himansu, S.-C. Chang, and P. C. E. Jorgenson, "Computation of a single airfoil gust response and gust-cascade interaction using the CE/SE method," in Proceedings of the Fourth Computational Aeroacoustics (CAA) Workshop on Benchmark Problems (2004).

[43]S. Jiang, "Investigation of gust-airfoil interaction noise," Doctoral dissertation (University of Southampton, 2022).

[44]B. A. Singer, K. S. Brentner, D. P. Lockard, and G. M. Lilley, "Simulation of acoustic scattering from a trailing edge," J. Sound Vib. **230**(3), 541 (2000).